Computer simulations of melts of ring polymers with nonconserved topology: A dynamic Monte Carlo lattice model

Mattia Alberto Ubertini [*] and Angelo Rosa [†]
Scuola Internazionale Superiore di Studi Avanzati (SISSA), Via Bonomea 265, 34136 Trieste, Italy

(Received 27 July 2021; revised 7 October 2021; accepted 26 October 2021; published 18 November 2021)

We present computer simulations of a dynamic Monte Carlo algorithm for polymer chains on a fcc lattice which explicitly takes into account the possibility to overcome topological constraints by controlling the rate at which nearby polymer strands may cross through each other. By applying the method to systems of interacting ring polymers at melt conditions, we characterize their structure and dynamics by measuring, in particular, the amounts of knots and links which are formed during the relaxation process. In comparison with standard melts of unknotted and unconcatenated rings, our simulations demonstrate that the mechanism of strand crossing makes polymer dynamics faster provided the characteristic timescale of the process is smaller than the typical timescale for chain relaxation in the unperturbed state, in agreement with recent experiments employing solutions of DNA rings in the presence of the type II topoisomerase enzyme. In the opposite case of slow rates the melt is shown to become slower, and this prediction may be easily validated experimentally.

DOI: 10.1103/PhysRevE.104.054503

I. INTRODUCTION

In dense polymer liquids and melts, the local Brownian motion of each polymer chain is subject to long-lived topological constraints (a.k.a. entanglements) imposed by the presence of the other chains. Well-documented manifestations of entangled polymer chain behavior include chains reptative motion in monodisperse melts of linear polymers [1–3] and chains spatial segregation in monodisperse melts of unknotted and unconcatenated ring polymers [4–7].

Polymer chains under typical dense conditions become mutually entangled because they are effectively uncrossable with each other [1,8]. In recent years, direct "manipulation" of entanglements in single chain molecules has opened new routes to fine-tune the mechanical properties of polymeric materials. This is, for instance, the case of the so-called *smart materials* like polycatenanes and polyrotaxanes [9,10], which are made of interlocked components whose internal degrees of freedom and mobility shape the unique conformational space of the molecule.

Interlocking and other topology manipulations are not exclusive to synthetic molecules; in fact, they take also a prominent role in the organization of the long DNA molecules which constitute the genomes of many organisms. For instance, in eukaryotic nuclei in normal cell conditions (interphase) the cm-long filament of DNA of each chromosome is densely packed into a corresponding μm-sized "territory" [11]. In this situation, tight confinement may result in an "excess" of entanglements which may be detrimental [12] at the later stage of cell division: a specific class of enzymes, the topoisomerases [13] and in particular the type II topoisomerase (hereafter, topoII), removes the entanglements [14] between two nearby DNA strands by cutting one strand, moving the other through the cut, and ligating the broken strand back.

Recently, Spakowitz's group at Stanford [15] showed that the "strand crossing" mechanism induced by the continuous action of topoII relaxes ("fluidizes") the topological constraints dominating the viscoelastic behavior of concentrated solutions of entangled DNA rings. Moreover, by blocking the activity of the enzyme, the once free rings become permanently linked with each other: under these conditions the DNA solution becomes equivalent to a so-called *Olympic gel*.

Theorized first by de Gennes [16,17], Olympic gels constitute a fascinating class of soft materials due to their remarkable theoretical [18–21], biological (the kinetoplast DNA of certain protozoa [22,23] can be modeled [24] as an Olympic gel), and even pharmacological [25] applications. The fundamental difference between an Olympic gel and a traditional gel is that the former is maintained together by topological bonds and not by chemical cross-links [8]. Studies like the one from Spakowitz's group demonstrate that it is indeed possible to change polymer topology to produce materials capable of switching from liquid-like to more solid-like behavior.

In this paper, we present the results of extensive numerical simulations describing the formation of linked networks of ring polymers in melt conditions. The work generalizes the efficient Monte Carlo scheme for lattice polymers described in Refs. [26,27] by expanding the set of stochastic moves in order to take explicitly into account the random occurrence of strand crossings between nearby polymer fibers.

By studying the behavior of melts of rings at different chain monomer numbers N and by comparing the systems in the presence and absence of strand crossings, we confirm that the strand crossing mechanism is capable of relaxing the effects of the topological constraints between different rings and enhance the overall mobility of the polymer fluid. On the other hand, this comes at the price of increasing the topological "complexity" of the chains in terms of links and knots. We

[*] mubertin@sissa.it
[†] anrosa@sissa.it

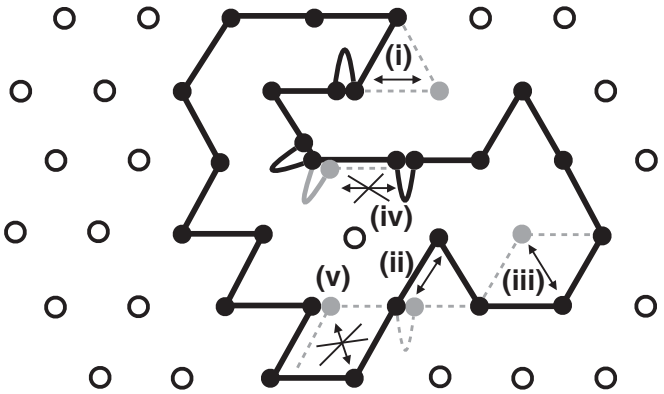

FIG. 1. Two-dimensional illustration of the lattice polymer model with topology-preserving moves. Monomers (filled dots) occupy the spatial positions of a regular lattice (empty dots) and two nearest-neighbor monomers are connected by a black line representing the polymer bond between them. For two nearest-neighbor monomers occupying the same lattice site the bond connecting them (the arcs) makes a unit of "stored length." Lattice positions connected by the double arrows are examples of MC *allowed* moves: (i) a unit of stored length unfolding to a normal bond, (ii) a bond folding into a unit of stored length, (iii) a Rouse-like move. Lattice positions connected by the double arrows with the cross are examples of MC *forbidden* moves: (iv) three consecutive monomers along the chain occupying the same lattice site, (v) two non-nearest-neighbor monomers violating the excluded volume constraint.

find that single chains swell with respect to the unknotted and unconcatenated ensemble, their average size increasing $\propto N^{1/2}$ as in ideal Gaussian rings: yet, we demonstrate that the stationary chain size is not equivalent to Gaussian and analyze in detail its structural and dynamical properties.

The paper is organized as follows. In Sec. II, we describe the polymer model, the numerical details of the algorithm, its computational cost and summarize the relevant length scales of the polymer melts. In Sec. III, we present the main results of the work. Then, in Sec. IV, we discuss an effect related to the efficiency of the strand crossing mechanism that may be tested in experiments employing DNA rings. The material presented here is complemented by additional figures in the Supplemental Material (SM) file [28].

II. THE POLYMER MODEL: SIMULATION PROTOCOL, LENGTH SCALES, METHODS

A. The kinetic Monte Carlo algorithm

We employ a kinetic Monte Carlo (MC) algorithm on the three-dimensional fcc lattice [29] with lattice spacing a corresponding to our unit of length, and we model solutions of ring polymers with *excluded volume* interactions.

The core of the algorithm is based on the elastic lattice polymer model inspired by Rubinstein's [30] repton model and developed in Refs. [26,27]. In this scheme (illustrated for simplicity in two dimensions in Fig. 1) two consecutive monomers along the chain either sit on nearest-neighbor lattice sites or they can be on the same lattice site: no more than two consecutive monomers may occupy the same lattice site, while nonconsecutive monomers are never allowed to occupy the same lattice site due to excluded volume. The bond length b between nearest-neighbor monomers takes then two possible values, a or 0; in the latter case the bond is said to host a unit of *stored length*. For a polymer with N bonds, the total contour length $L \equiv N\langle b\rangle < Na$ where $\langle b\rangle$ is the average bond length. This numerical trick makes the polymer elastic.

The dynamic evolution of the chains is implemented by combining two kinds of MC moves, which we classify based on the effects they produce on the global topology of the chain: (i) topology-preserving moves (Sec. II A 1) and (ii) topology-changing by stochastic strand crossing moves (Sec. II A 2).

1. Topology-preserving moves

The first set of MC moves is as in the original lattice model [26,27]: by construction, these moves preserve the overall topological state of the system. They consist in randomly picking a monomer of one of the chains in the system and attempting its displacement towards one of the nearest lattice sites (see Fig. 1 for a schematic illustration of these moves). The move is accepted if chain connectivity is preserved and with the additional constraints that (1) either the destination lattice site is empty or (2) the lattice site is occupied by only one of the nearest-neighbor monomers along the chain. In analogy with classical [1,8] polymer dynamics, case (1) is an example of a *Rouse*-like move while case (2) is a *reptation*-like move (essentially the move produces mass drift along the contour length of the chain, as occurs in reptation dynamics). It is easy to see that, at low polymer densities, most of the lattice sites are empty and Rouse moves prevail over reptation, while in the opposite case of high polymer densities, reptation becomes the dominant mode through which polymer chains relax. Therefore the algorithm reproduces known [1,8] features of polymer dynamics and, thanks to the stored length "trick" which integrates local fluctuations of the chain density, remains efficient even when it is applied to the equilibration of very dense systems [27].

2. Topology-changing (strand crossing) moves

Here we are interested in studying melts of ring polymers where topology changes are induced over time. In particular we consider the basic mechanism of *strand crossing* (hereafter, SC) involving a pair of nearby polymer filaments, similar to the action triggered by the enzyme topoII in DNA ring solutions [15].

As explained in Sec. II A 1, the original [26,27] lattice model does not include such a feature: we show here that it is, however, possible to remove this "constraint" and we describe the simplest possible MC move capable of inducing a single crossing between two nearby polymer strands. These polymer strands may either belong to the same chain (*intrachain* SC) or they can stay on two distinct chains (*interchain* SC).

The new move (which is also one of the main contributions of this paper [31]) is explained with the help of the two examples in Fig. 2. Take the two distinct polymer strands, each of effective contour length $2a$, which are illustrated, in each panel of the figure, as the thicker portions of the two closed curves. The two segments are chosen with the constraints that the corresponding central monomers (the bigger dots) (i) are positioned at lattice site distance a and (ii) one can switch position with the other and be then reconnected to the other

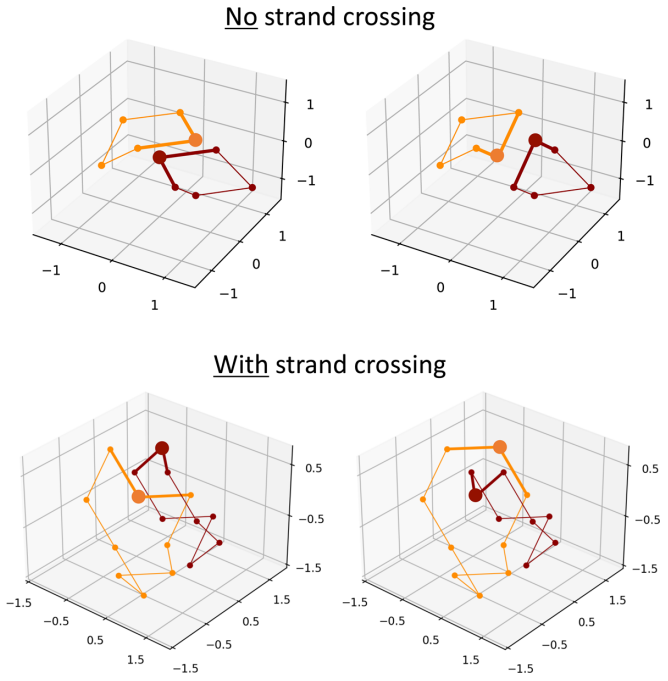

FIG. 2. Illustration of Monte Carlo moves for strand crossing. On each pair [red or orange (color) or dark or light gray (black and white)] of ring polymers we identify those portions (the thicker strands) of contour length $2a$ whose central monomers (the bigger dots) are one lattice site far apart. The two strands can be "transformed," such that the original central monomer of one strand turns into the central monomer of the other strand (left-hand-side panels vs right-hand-side panels) and vice versa, without violating the chain connectivity constraint. In some cases (e.g., as in the top row) this operation does not lead to strand crossing, in others (e.g., as in the bottom row) it does. We list all cases (12 in total) leading to strand crossing and implement them in our MC algorithm. The configurations in the bottom row constitute an example of a linking (left → right) or an unlinking (right → left) event.

chain with no violation of polymer connectivity and preserving the contour length. By exhaustive search, we have then compiled the list of all possible (36 in total) swapping moves compatible with these constraints. By closer examination, we verify that 24 of them do not produce SC (essentially the two chain strands remain on parallel planes even after swapping, see the polymer configurations in the top row in Fig. 2), while the remaining 12 moves effectively lead to a single SC (as in the polymer configurations in the bottom row in Fig. 2). The successful SC has been verified by looking at the *variation*, $|\Delta\mathcal{G}| = +1$, of the *Gauss linking number* $\mathcal{G}$ [see definition, Eq. (11)] relative to the piecewise closed curves formed by the triplets of monomers involved in the MC swapping move.

The implementation of this move in the kinetic MC algorithm is as follows: We pick randomly two polymer strands of effective contour length $2a$ and then check whether they belong to the set compatible with a SC and, if so, we swap the corresponding central monomers. When the two involved strands belong to the same ring, the move is introducing *knots* in the chain (Sec. III A 3), while on two separate rings it will induce the formation of *links* (Sec. III B).

B. Simulation details

We have considered bulk solutions of M closed (ring) polymer chains, each chain made of N monomers or bonds. With values $N \times M = [40 \times 5120,\ 80 \times 2560,\ 160 \times 1280,\ 320 \times 640,\ 640 \times 320]$ each system contains a fixed number of monomers, 204 800. Bulk conditions are implemented through the enforcement of periodic boundary conditions in a simulation box of total volume $V = L^3$, where the linear size of the box, L, has been fixed based on the monomer number density $\rho a^3 \equiv \frac{NM}{V} a^3 = 1.23$ corresponding to melt conditions [27,32].

We have studied and compared structure and dynamics for different setups:

1. Ring polymer melts with *nonconserved* chain topology. Here, the topological state of the system changes in time according to the SC mechanism. Therefore, the MC scheme includes the whole set of dynamic moves described in Secs. II A 1 and II A 2.

2. Ring polymer melts with *conserved* chain topology. Here, only moves from Sec. II A 1 are included. Since now topology cannot relax, the choice of the initial state is crucial. The following two options have been considered: (i) Equilibrated melts of *unknotted and unconcatenated* or (for brevity and as in Ref. [32]) *untangled* rings. (ii) Equilibrated melts of *permanently catenated* rings, corresponding to the equilibrated polymer conformations obtained at the end of the simulations with nonconserved chain topology. The name anticipates some properties of the rings (catenation and linking) that will be discussed in depth in Sec. III B.

3. For additional comparison, we have also considered ideal (i.e., no excluded volume and no topological interactions) rings.

At each MC time step, monomers are picked at random and time is measured in MC units of $\tau_{\rm MC} \equiv NM$. For polymer solutions with nonconstrained topology (Sec. II A 2) one needs to specify also the *rate* $\lambda_{\rm SC}$ at which SCs occur. In principle, this rate is a free parameter of our model that we must tune. For the typical experimental conditions described in the work by Spakowitz *et al.* [15], it was estimated that the action rate of topoII on DNA rings is close to its *intrinsic* rate of $O(1\ {\rm s}^{-1})$ and $\approx 10^4$ times slower than the mean diffusion time of a single DNA persistence length. Considering that our polymers are pretty flexible (see Sec. II E), we take here one SC move (modeled according to Sec. II A 2) each 10^4 MC time steps (i.e., $\lambda_{\rm SC}^{-1} = 10^4 \tau_{\rm MC}$) with only topology-preserving moves. Notice that the algorithm makes the implicit assumption that the enzyme topoII is immediately available for the reaction, i.e., the SC process is intrinsically *reaction-limited*. Nonetheless, we will also discuss (see Sec. IV) smaller values of $\lambda_{\rm SC}$ corresponding to "less efficient" topoII.

Figure 3 shows that the algorithm generates the correct dynamics. By taking the longest rings with $N = 640$, the diffusive monomer [Fig. 3(a)] and chain [Fig. 3(b)] motions for the three cases of melts of (i) untangled rings, (ii) rings with active SCs, and (iii) permanently catenated rings nicely superimpose on each other on timescales shorter than the SC timescale $\lambda_{\rm SC}^{-1}$, i.e., ring dynamics on these timescales is not sensitive to SCs and deviates above $\lambda_{\rm SC}^{-1}$. Importantly, this test confirms that the local segment dynamics is not significantly

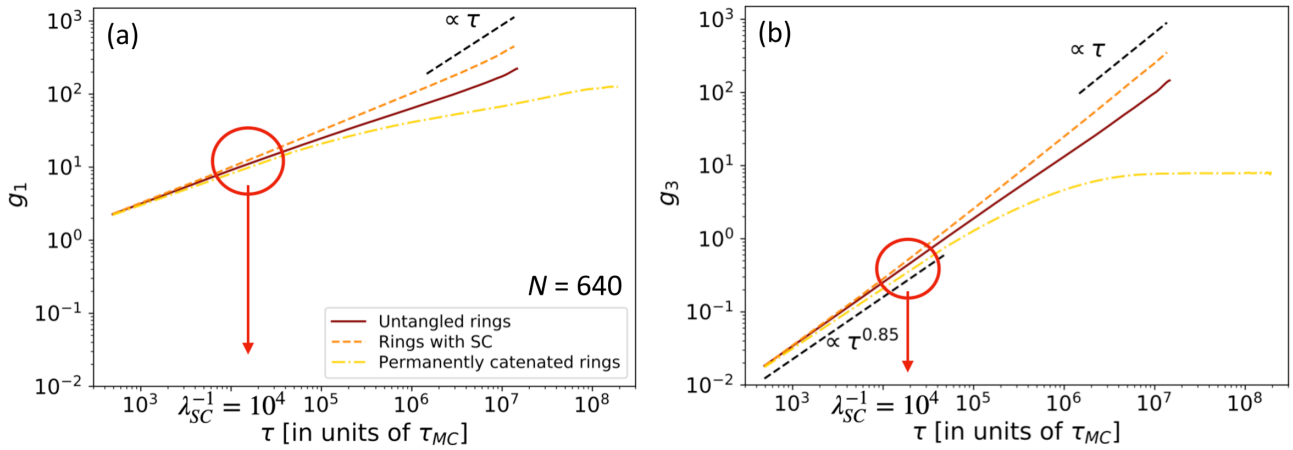

FIG. 3. Time mean-square displacements of (a) single chain monomers $[g_1(\tau) \equiv \langle[\vec{r}_{\rm mon}(t+\tau) - \vec{r}_{\rm mon}(t)]^2\rangle]$ and (b) the chain center of mass $[g_3(\tau) \equiv \langle[\vec{r}_{\rm c.m.}(t+\tau) - \vec{r}_{\rm c.m.}(t)]^2\rangle]$ for rings with $N = 640$ monomers. Here, $\vec{r}_{\rm mon}(t)$ and $\vec{r}_{\rm c.m.}(t)$ are the spatial positions for the single monomer and center of mass of the chain respectively, and brackets denote ensemble and time averages. In both panels, the lines for (i) melts of untangled rings (red, solid), (ii) rings with active SCs (orange, dashed), and (iii) permanently catenated rings (yellow, dot-dashed) visibly depart (circle) from each other at the imposed SC timescale $\lambda_{\rm SC}^{-1}/\tau_{\rm MC} = 10^4$ (see Sec. II B).

altered by the presence of SCs (see Sec. II C for more details on this point).

C. Comparison with other simulation methods

In this section, we review some computational work having significative overlap with (i) our method of creating strand crossings and (ii) the consequent formation of linked gels from melts of entangled rings.

In two papers [33,34], Schaffer introduced and studied the physical properties of a Monte Carlo model for polymer dynamics where monomers have distinct positions on the simple cubic lattice and bonds are allowed to fluctuate by inclusion of the first, second, and third nearest neighbors of each monomer. Chain dynamics proceeds by random monomer displacements which respect bond constraints and excluded volume. Then, topological constraints between different chains are switched on (off) by forbidding (allowing) chain conformations with bonds which may cross at their midpoints. Using these simple rules, the model was applied first to melts of linear chains [33,34] and later on to melts of untangled rings and rings with SCs [35]. Our results for ring structure (see Sec. III A 1) and dynamics (see Sec. III B 2) substantially confirm the results reported in Ref. [35].

An approach very similar to Schaffer's was then employed by Lang and coworkers in a series of more recent papers [18–21]: specifically, the authors complemented the *bond fluctuation* model on the fcc lattice [36,37] with a set of *diagonal* moves (the so-called "x traps" [38]), which enforce the temporary overlap of polymer bonds and hence possible SCs. The model was used to study the conformational properties of Olympic gels, however the dynamics of the gel was not discussed.

The philosophy at the basis of these two models is the same: letting random overlaps between bonds as the first, necessary, step for strand crossings to occur. However (quoting Schaffer [33]), this procedure suffers from the inconvenience that "the local density is not guaranteed to be the same ... because the noncrossing simulations exclude a small fraction of configurations (those in which bond midpoints overlap) that are included in the crossing simulations." At the same time, albeit small, the chain local mobility changes in moving from noncrossing to crossing simulations (Ref. [33], Fig. 5) and the corresponding single-monomer time mean-square displacements $g_1(\tau)$ do not coincide at short timescales (see figure 8 in Ref. [33]) where we expect the effects of SCs to be small.

For the completeness of the discussion, it is worth mentioning that the preservation of the local density may indeed be a problem that one has to deal with also in classical off-lattice simulations. Related to that, in Ref. [24] Michieletto and coworkers used classical Brownian dynamics simulations of a bead-spring polymer model to construct model Olympic gel conformations for the DNA kinetoplast. In this study, entanglements were removed by (i) switching off the nonbonded monomer-monomer interactions of the system, (ii) letting the system equilibrate, and (iii) slowly turning interactions on again. However, as demonstrated by Auhl *et al.* [39], this procedure must be performed with extreme care, especially when applied to dense polymer solutions because it may lead to considerable artifacts if the system is not allowed to equilibrate properly.

Clearly both problems discussed above (the nonpreservation of the local density *and* chain mobility) are absent in our work, see Figs. 2 and 3(a). At the same time, the protocol allows for easy calibration of the relevant SC parameter $\lambda_{\rm SC}$ (Sec. II B) whose effects are considered here (see Discussion, Sec. IV).

D. Computing observables for polymer structure

The ensemble-average value, $\langle\mathcal{O}\rangle$, for the generic single-chain observable $\mathcal{O}$ is given by the mathematical expression:

$$\langle\mathcal{O}\rangle \equiv \frac{1}{M}\sum_{m=1}^{M}\frac{1}{T_{\rm run}-\tau_d}\int_{\tau_d}^{T_{\rm run}}\mathcal{O}_m(t)dt, \qquad (1)$$

TABLE I. Computational cost of MC runs. In interacting systems (melts), M is the total number of chains, whereas for ideal systems with no excluded volume interactions it represents the number of single independent runs. (i) $T_{\rm run}$: length of the single MC run. (ii) τ_d: ring self-diffusion time. Values for permanently catenated rings with $N = 320$ and $N = 640$ are not defined because the corresponding time mean-square displacements of the center of mass [$g_3(\tau)$, Eq. (17)] attain the characteristic plateaus for stacked dynamics [see Fig. 9(c)]. $\tau_{\rm MC} = NM$ is the Monte Carlo time unit (see Sec. II B for details).

N	M	$T_{\rm run}[\tau_{\rm MC}]$	$\tau_d[\tau_{\rm MC}]$
		Ideal rings	
40	100	$\simeq 6.0 \times 10^6$	$\simeq 7.0 \times 10^3$
80	100	$\simeq 6.0 \times 10^6$	$\simeq 7.0 \times 10^3$
160	100	$\simeq 6.0 \times 10^6$	$\simeq 1.0 \times 10^4$
320	100	$\simeq 9.0 \times 10^6$	$\simeq 4.0 \times 10^4$
640	200	$\simeq 1.5 \times 10^7$	$\simeq 2.0 \times 10^5$
		Melts of untangled rings	
40	5120	$\simeq 2.0 \times 10^6$	$\simeq 1.0 \times 10^4$
80	2560	$\simeq 2.0 \times 10^6$	$\simeq 3.0 \times 10^4$
160	1280	$\simeq 2.0 \times 10^6$	$\simeq 2.0 \times 10^5$
320	640	$\simeq 4.0 \times 10^6$	$\simeq 7.0 \times 10^5$
640	320	$\simeq 1.5 \times 10^7$	$\simeq 3.0 \times 10^6$
		Melts of rings with strand crossings	
40	5120	$\simeq 2.0 \times 10^6$	$\simeq 1.0 \times 10^4$
80	2560	$\simeq 2.0 \times 10^6$	$\simeq 3.0 \times 10^4$
160	1280	$\simeq 2.0 \times 10^6$	$\simeq 1.0 \times 10^5$
320	640	$\simeq 5.0 \times 10^6$	$\simeq 6.0 \times 10^5$
640	320	$\simeq 1.4 \times 10^7$	$\simeq 2.0 \times 10^6$
		Melts of permanently catenated rings	
40	5120	$\simeq 2.0 \times 10^6$	$\simeq 1.0 \times 10^4$
80	2560	$\simeq 2.0 \times 10^6$	$\simeq 5.0 \times 10^4$
160	1280	$\simeq 7.0 \times 10^6$	$\simeq 5.0 \times 10^5$
320	640	$\simeq 9.8 \times 10^7$	
640	320	$\simeq 1.9 \times 10^8$	

where $\mathcal{O}_m(t)$ is the value of the observable calculated for the mth ring at time t and $T_{\rm run}$ is the total runtime of the MC trajectory (values for $T_{\rm run}$, illustrating the computational cost of our simulations, are reported in Table I). The time average in Eq. (1) is calculated by discarding the initial portion of each trajectory which is of the order of the self-diffusion time [$\tau_d(N)$, see values in Table I] of the polymers. $\tau_d(N)$ corresponds to the timescale for the polymer to diffuse of a distance the size of its own mean gyration radius, $g_3(\tau_d(N)) \equiv \langle R_g^2(N)\rangle$, where $g_3(\tau)$ is the time mean-square displacement of the chain center of mass [see definition, Eq. (17)].

E. Polymer model: Length scales

For completeness, here we give a few additional details about the relevant length scales (summarized in Table II) used to characterize the local bending and the entanglement properties of polymer melts. We remind the reader that, as in Refs. [27,32], we choose the monomer number density $\rho = 1.23a^{-3}$ where a is the fcc lattice unit distance (Sec. II A).

TABLE II. Values of physical parameters for melts of ring polymers on the fcc lattice with unit distance a and monomer number density $\rho a^3 = 1.23$: (i) $\langle b\rangle$, mean bond length; (ii) ℓ_K, Kuhn length [Eq. (2)]; (iii) $\rho_K \ell_K^3$, number of Kuhn segments per Kuhn volume [40]; (iv) L_e, entanglement length [Eq. (4)]; (v) $N_e \equiv L_e/\langle b\rangle$, number of bonds per entanglement length.

$\langle b\rangle/a$	ℓ_K/a	$\rho_K \ell_K^3$	L_e/ℓ_K	N_e
0.74	1.48	1.9937	100.633	201.266

Average bond length $\langle b\rangle$. Due to excluded volume effects and chain packing the average bond length $\langle b\rangle = 0.74a < a$.

Kuhn length ℓ_K. The Kuhn length is used to quantify the flexibility of polymer chains [1,8]. Given the mean-square end-to-end distance $\langle R^2(\ell)\rangle$ between monomers at contour length separation ℓ on *linear* chains, ℓ_K is defined as [1,8]:

$$\ell_K \equiv \lim_{\ell\to\infty} \frac{\langle R^2(\ell)\rangle}{\ell}, \tag{2}$$

provided that such a limit exists [41]. To determine the polymer Kuhn length of our polymer chains, we simulated systems of $M = 640$ linear chains with $N = 320$ monomers per chain and with chain dynamics as described in Sec. II A 1. After equilibration, we computed the ratio [Eq. (2)] $\frac{\langle R^2(\ell)\rangle}{\ell}$, where $\ell = n\langle b\rangle$ is the contour length separation between any two monomers separated by n bonds along the chain. We have found that this quantity gives a plateau in the region $\ell = [200\langle b\rangle, 300\langle b\rangle]$ whose value, estimated by best fit to a constant, is reported in Table II. For completeness, the same procedure applied to ideal polymers leads to $\ell_K \simeq 1a$, i.e., ideal polymers are locally more flexible than interacting polymers.

Entanglement length L_e. Dense untangled rings are known [4,7,42] to compact above a characteristic length scale, which is the entanglement length L_e of the chains. According to the classical packing argument by Lin [43] and by Kavassalis and Noolandi [44], the number of entanglement strands inside the volume spanned by a single entanglement volume,

$$\frac{\rho_K}{L_e/\ell_K} \langle R^2(L_e)\rangle^{3/2} \simeq 20, \tag{3}$$

is a universal constant. In Eq. (3), ρ_K is the number density of Kuhn segments and $\langle R^2(L_e)\rangle = \ell_K L_e$ is the mean-square end-to-end distance of a linear polymer chain of contour length $=L_e$ [Eq. (2)]. Equation (3) is then equivalent to

$$\frac{L_e}{\ell_K} \simeq \left(\frac{20}{\rho_K \ell_K^3}\right)^2, \tag{4}$$

i.e., the ratio L_e/ℓ_K is a function of the number of Kuhn segments inside the (Kuhn) volume $=\ell_K^3$. By using Eq. (4) it is a simple exercise to extract L_e/ℓ_K and the corresponding number of monomers per entanglement length, N_e. In particular, we notice that the largest rings with $N = 640 \approx 3N_e$ are above the entanglement threshold and are expected [4,7,42] to crumple due to topological constraints.

TABLE III. Single-chain properties in melts of N-monomer rings. (i) $\langle R_g^2 \rangle$: ring mean-square gyration radius, expressed in lattice units. (ii) $P_{\rm knot}$: mean knotting probability per chain (only for melts of rings with strand crossings).

N	$\langle R_g^2 \rangle / a^2$	$P_{\rm knot}$
	Ideal rings	
40	3.178 ± 0.002	
80	6.284 ± 0.006	
160	12.52 ± 0.02	
320	24.9 ± 0.1	
640	50.0 ± 0.3	
	Melts of untangled rings	
40	3.3334 ± 0.0004	
80	6.361 ± 0.003	
160	11.88 ± 0.02	
320	21.9 ± 0.1	
640	38.1 ± 0.5	
	Melts of rings with strand crossings	
40	3.5093 ± 0.0005	0
80	7.088 ± 0.004	1×10^{-3}
160	14.30 ± 0.02	6×10^{-3}
320	28.6 ± 0.1	3×10^{-2}
640	57.6 ± 0.4	9×10^{-2}
	Melts of permanently catenated rings	
40	3.521 ± 0.004	
80	7.10 ± 0.01	
160	14.36 ± 0.07	
320	29.3 ± 0.3	
640	59 ± 1	

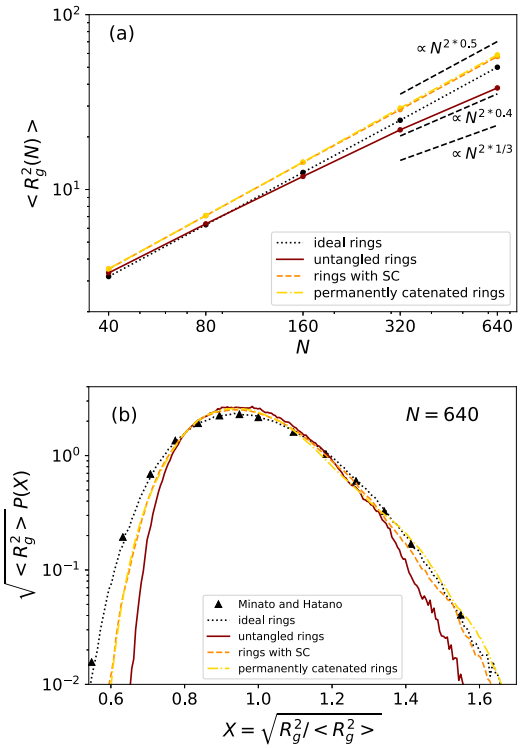

FIG. 4. (a) Mean-square gyration radius of ring polymers, $\langle R_g^2(N) \rangle$, as a function of the number of bonds, N (for detailed values at each N, see Table III). Different colors and line styles are for different polymer ensembles (color code and line styles for untangled rings, rings with SC, and permanently catenated rings are as in Fig. 3), and dashed lines correspond to theoretical asymptotic behavior. (b) Distribution functions of gyration radius, $P(R_g/(\langle R_g^2 \rangle)^{1/2})$, in the different ring ensembles and for the largest chains ($N = 640$). The up-triangles correspond to Minato and Hatano's exact analytical result for ideal rings [45].

III. RESULTS

A. Single-chain structure

1. Ring size

We have studied first how the average ring size, or the polymer mean-square gyration radius

$$\langle R_g^2(N) \rangle \equiv \frac{1}{N} \sum_{i=1}^{N} \langle (\vec{r}_i - \vec{r}_{\rm c.m.})^2 \rangle \sim N^{2\nu}, \tag{5}$$

scales as a function of N. In Eq. (5), $\vec{r}_i$ are the monomer coordinates, $\vec{r}_{\rm c.m.}$ is the chain center of mass, and ν is the Flory scaling exponent [8]. The results for the different ensembles are summarized in Table III and plotted in Fig. 4(a).

In agreement with Refs. [5,7,32], topological constraints in untangled melts are ineffective below $N \lesssim N_e$ where $N_e \approx 200$ is the total number of monomers per entanglement length (see Sec. II E). Above N_e, the mutual topological constraints between nearby rings let the chains to deviate from the ideal behavior $\langle R_g^2(N) \rangle \sim N^{2\times 1/2}$ and to become more compact: in particular here we report the scaling $\langle R_g^2(N) \rangle \sim N^{2\times 0.4}$, which describes [4] the slow crossover to the asymptotic compact regime $\langle R_g^2(N) \rangle \sim N^{2\times 1/3}$ [6,7]. In the presence of active SCs the rings swell again, $\langle R_g^2 \rangle \sim N^{2\times 1/2}$, and reach a steady state which does not change further after the SC mechanism is switched off and rings become permanently catenated [overlying dashed and dot-dashed lines in Fig. 4(a)].

It is interesting to point out that, while the reported scaling exponent $\nu = 1/2$ is the same of ideal chains, rings structure remains nonetheless nonideal. To show that, we have computed the complete distribution function, $P(R_g)$, of the gyration radius and compared their shapes in the different ensembles [see Fig. 4(b) for the particular case $N = 640$ and Fig. S1 in the SM [28] for rings of different values of N]. First, ideal rings [dotted line in Figs. 4(b) and S1(a)] are remarkably well described by the analytical expression [up-triangles in Fig. 4(b) and dashed line in Fig. S1(a) in the SM [28]] by Minato and Hatano [45]. Second, untangled rings [solid lines in Figs. 4(b) and S1(b) in the SM [28]] show systematic deviations from the ideal behavior which are especially visible for small and large values of R_g. Third, rings with active SCs and permanently catenated rings have, as expected, the same $P(R_g)$ [dashed and dot-dashed lines in Figs. 4(b) and in Figs. S1(c) and S1(d) in the SM [28]]: the curves are consistent with ideal behavior only for large values of R_g, while for small values of R_g they confirm the nonideal nature of rings and highlight the incomplete screening of excluded volume at short scales.

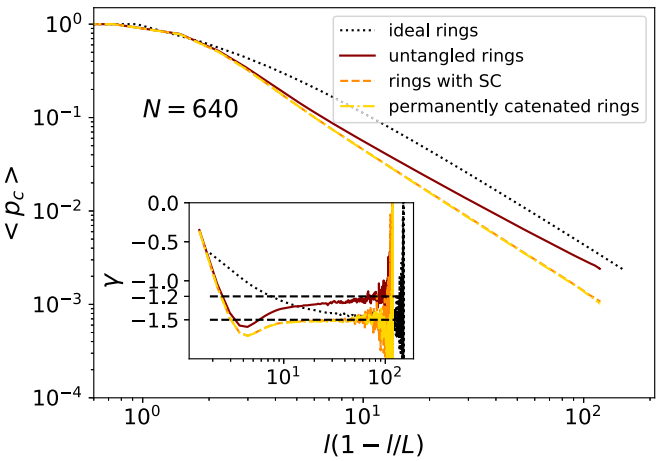

FIG. 5. Monomer-monomer mean contact probability $\langle p_c(\ell)\rangle_L$ as a function of $\ell(1-\ell/L)$ and for the largest simulated rings ($N \equiv L/\langle b\rangle = 640$) in the different ensembles. We define two monomers to be in contact if their distance is $\leqslant$ one lattice unit. (inset) Local scaling exponent $\gamma(\ell)$, defined as the logarithmic derivative of $\langle p_c(\ell)\rangle_L$ [Eq. (6)]. Dashed horizontal lines correspond to theoretical asymptotic behavior. Color code and line styles are as in Fig. 4.

2. Contact probabilities

We investigate the physics of polymer self-interactions and consider the mean contact probability $\langle p_c(\ell)\rangle_L$ between pairs of monomers separated by n bonds (equivalent to the mean contour length $\ell = n\langle b\rangle$, see Table II) for rings of total mean contour length $L \equiv N\langle b\rangle$. $\langle p_c(\ell)\rangle$ appears frequently in studies related to DNA-DNA interactions in chromosome conformation capture experiments [46–48].

In agreement with Ref. [49], finite-chain effects can be reduced and the universal shape of $\langle p_c(\ell)\rangle_L$ in the large-L limit can be demonstrated by plotting the curves for different values of L in terms of the variable $\Lambda = \ell(1-\ell/L)$ (see Fig. S2 in the SM [28]). It is then useful to discuss the scaling behavior of $\langle p_c(\ell)\rangle_L$ by introducing the local exponent

$$\gamma(\ell) \equiv \frac{d\ln\langle p_c(\ell)\rangle_L}{d\ln\Lambda}. \tag{6}$$

Figure 5 shows results for $\langle p_c(\ell)\rangle_L$ (main) and the corresponding $\gamma(\ell)$ (inset) for rings with $N = L/\langle b\rangle = 640$ in the different ensembles. Asymptotically, ideal rings, rings with SCs, and permanently catenated rings converge all to the ideal value $\gamma = -\frac{3}{2}$ while untangled rings show $\gamma \simeq -1.2$, consistent [50] with $\nu \simeq 0.4$ (Fig. 4) for these systems. On the contrary, and quite interestingly, the small scale behavior of $\gamma(\ell)$ for rings with SCs is strongly *nonideal*, in agreement with the similarly nonideal behavior seen for the corresponding chain size distributions [Fig. 4(b)].

3. Knot statistics in ring polymers with strand crossings

Topological constraints in untangled melts make the chains more compact with respect to the ideal case, a situation which is radically altered in the presence of active SCs [Fig. 4(a)]. SCs act in the same way regardless of whether the two strands are on the same or on different rings (see Sec. II A 2): for this reason they change both single-chain topology by forming *knots* and interchain topology by forming *links* (studied in Sec. III B).

There exists copious literature on the effects of physical knots (and links) in polymer filaments and soft matter, see the review work [51]. Knots in closed curves can be classified based on the number of *irreducible* crossings they present when one tries to smoothly deform the curve so as to force it to lie on a plane [51,52]: neglecting chirality, there exist one single knot with three crossings (3_1, the trefoil knot), one with four (4_1, the figure-eight knot), two with five crossings (5_1 and 5_2), etc. In general, at increasing knot complexity, the same number of crossings correspond to several topologically distinct knot types.

In general, knots classification is carried out by means of suitable *topological invariants*. One of the simplest and most popular of the knot invariants, which we also adopt in the present work, is given by the so-called Alexander polynomial [51,52] of the knot, which provides a mathematically tractable representation of the smallest number of chain crossings occurring in the closed curve. Here, we used the open package KymoKnot [53] to detect and classify first the knots which form in our polymer chains through SC. Then, for simplicity, we used the sole number of irreducible crossings, $\mathcal{K}$, for knot classification, i.e., knots like the already-mentioned 5_1 and 5_2 fall into the same group $\mathcal{K} = 5$. An example of a model ring conformation entrapping a trefoil knot is given in Fig. 6(a).

Figure 6(b) shows the probability $P(N;\mathcal{K})$ that N-monomer rings have given knot type $\mathcal{K} = 0$ (the unknot), $\mathcal{K} = 3$ (the trefoil, i.e., the simplest nontrivial knot) and so on for knots of increasing complexity. Knots of complex shapes are in general rare (the trefoil dominates), yet their frequency increases [51,52] steadily with N and for $N = 640$ we are even able to detect a few, and quite complex, knotted structures up to 11 crossings.

Then we consider the cumulative knotting probability, defined as

$$P_{\rm knot}(N) \equiv \sum_{\mathcal{K}=3,4,\ldots} P(N;\mathcal{K}) = 1 - P(N;\mathcal{K}=0). \tag{7}$$

In Ref. [18], Lang and coworkers showed that for catenated N-monomer rings in solution $P(N;{\rm kt}=0_1) \simeq \exp(-N/N_0)$, where N_0 is some characteristic (and model dependent [54]) polymer length scale. The exponential character of $P(N;\mathcal{K}=0)$ matches the known conjecture [52,54] that the probability of the unknot in *ideal*, closed lattice polygons decays exponentially with the chain contour length, and it implies that $P_{\rm knot}(N)$ has a *concave* shape when displayed in a lin-lin plot. Our data for $P_{\rm knot}(N)$ do not seem to reflect this behavior, they are better described instead by the simple power law [see symbols vs line in the left-hand-side (l.h.s.) inset (lin-lin plot) and the right-hand-side (r.h.s.) inset (log-log plot) of Fig. 6(b)]:

$$P_{\rm knot}(N) = \left(\frac{N}{N_{\rm knot}}\right)^{\alpha_{\rm knot}}, \tag{8}$$

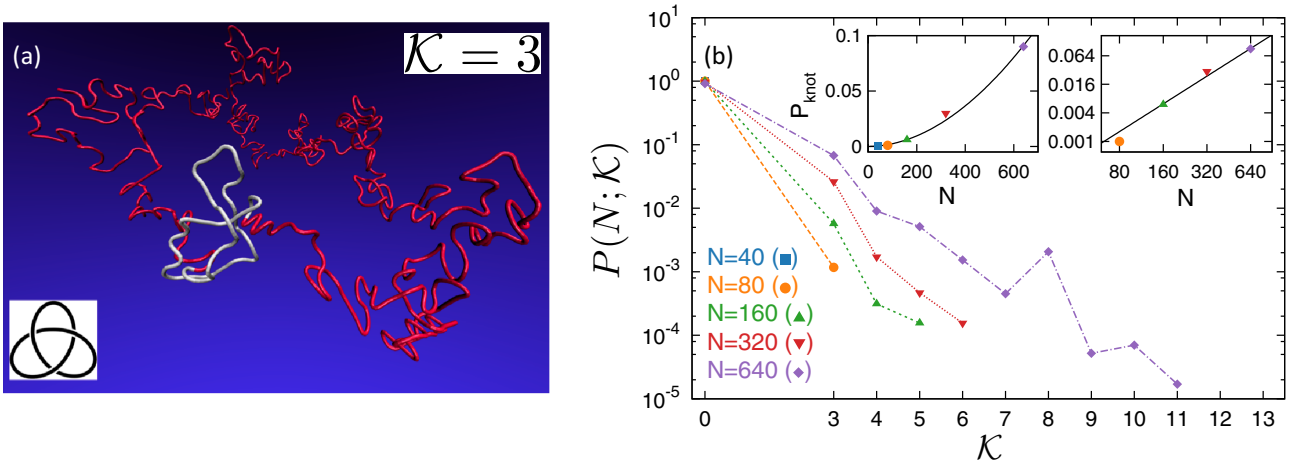

FIG. 6. (a) Model conformation of a ring polymer (in red) entrapping a trefoil ($\mathcal{K} = 3$) knot (highlighted in white). (b) Probability distribution function $P(N;\mathcal{K})$ of knots with $\mathcal{K}$ crossings in N-monomer rings (different symbols and line styles correspond to different values of N) undergoing continuous SCs. Rings with $N = 40$ do not knot during the simulation. The two insets show plots [in lin-lin (left) and log-log (right) representations] of the knotting probability $P_{\rm knot}$, Eq. (7), as a function of N (symbols) and the corresponding best fit to power-law behavior [line, Eq. (8) with Eqs. (9) and (10)].

with [55]

$$N_{\rm knot} = 2203 \pm 433, \tag{9}$$

$$\alpha_{\rm knot} = 1.9 \pm 0.2. \tag{10}$$

Of course it is possible that the quadratic behavior, Eqs. (8) and (10), is just a crossover to the "$\sim 1 - \exp(-N/N_0)$" behavior and that we cannot detect the latter because polymers of higher N need to be considered. Yet, it is interesting to notice that the value $\alpha_{\rm knot} \approx 2$ [Eq. (10)] has a simple interpretation: it mirrors the enforced mechanism where knots form "cooperatively" due to random SCs between pairs of polymer strands.

Another possible explanation for the discrepancy between the results by Lang *et al.* [18] and Eqs. (8) and (10) may come from the different ways the SCs are generated in the two models. Lang *et al.* used the bond fluctuation model [36,37] with the addition of a set of diagonal moves which switch temporarily off all the entanglements (see comments in Sec. II C): in this sense, their SC mechanism reproduces somehow the features of an ideal polymer and for this reason the reported knotting probability decays exponentially according conjecture [52,54]. Our ring polymers, instead, remain not ideal [Fig. 4(b)]: simply, the physical entanglements emerging from the uncrossability [1,8] of the chains are resolved by a dynamic mechanism which does not require chain-chain overlap (Fig. 2).

In conclusion, to assess the validity of Eq. (8) systematic (and computationally much more expensive) simulations of polymers of higher values of N need to be done; in particular, since $P_{\rm knot}(N) \to 1$ for large N, we expect rings with $N \gtrsim N_{\rm knot}$ to be always knotted on average.

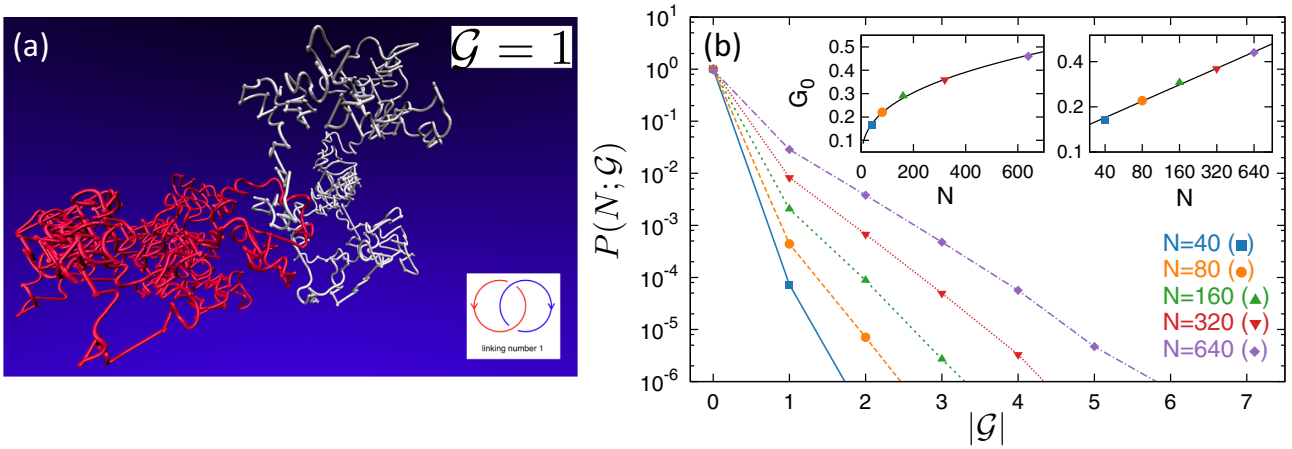

FIG. 7. (a) Pair of model ring conformations connected by a link with Gauss linking number [Eq. (11)] $\mathcal{G} = 1$. (b) Probability distribution function $P(N;|\mathcal{G}|)$ of the absolute value $|\mathcal{G}|$ of the Gauss linking number between pairs of N-monomer rings. The two insets show plots [in lin-lin (left) and log-log (right) representations] of the decay length $\mathcal{G}_0$ vs N [symbols, Eq. (12)] and best fit to power-law behavior [line, Eq. (13) with Eqs. (14) and (15)]. Color code, line styles and symbols are as in Fig. 6(b).

TABLE IV. Network properties in melts of N-monomer rings with strand crossings. (i) $\mathcal{G}_0$: decay length for the probability distribution function of the Gauss linking number, $P(N;\mathcal{G}) \sim e^{-|\mathcal{G}|/\mathcal{G}_0(N)}$ (see Fig. 7(b) and Fig. S3 in the SM [28]). (ii) $\langle \mathrm{LD} \rangle$: mean linking degree. (iii) p_{link}: mean fraction of pairs of linking rings.

N	$\mathcal{G}_0$	$\langle \mathrm{LD} \rangle$	p_{link}
40	0.164 ± 0.004	0.376 ± 0.001	$(7.32 \pm 0.02) \times 10^{-5}$
80	0.22 ± 0.01	1.143 ± 0.003	$(4.46 \pm 0.01) \times 10^{-4}$
160	0.29 ± 0.01	2.754 ± 0.004	$(2.153 \pm 0.003) \times 10^{-3}$
320	0.36 ± 0.01	5.77 ± 0.01	$(9.00 \pm 0.02) \times 10^{-3}$
640	0.46 ± 0.01	10.92 ± 0.08	$(3.29 \pm 0.02) \times 10^{-2}$

B. Structure and dynamics of ring polymers with strand crossings

1. Physical links

The physical links between any given pair of rings $\mathcal{R}_1$ and $\mathcal{R}_2$ have been quantified in terms of the corresponding *Gauss linking number* [51,52]:

$$\mathcal{G} \equiv \frac{1}{4\pi} \oint_{\mathcal{R}_1} \oint_{\mathcal{R}_2} \frac{(\vec{r}_2 - \vec{r}_1) \cdot (d\vec{r}_2 \wedge d\vec{r}_1)}{|\vec{r}_2 - \vec{r}_1|^3}, \tag{11}$$

where $\vec{r}_1$ (respectively, $\vec{r}_2$) is the spatial coordinate for a point on the (oriented) contour line formed by ring $\mathcal{R}_1$ (resp., ring $\mathcal{R}_2$) and $d\vec{r}_1$ (resp., $d\vec{r}_2$) is the corresponding infinitesimal increment. As in the case of the Alexander polynomials (used in Sec. III A 3), $\mathcal{G}$ is also a *topological invariant*: physically, it represents the number of times (with "+" or "−" sign, depending on the reciprocal orientations of the curves) that each curve winds around the other. For our rings modeled as discretized closed paths on the $3d$ fcc lattice, Eq. (11) has been evaluated numerically by employing the efficient algorithm by Klenin and Langowski [56]. An example of a pair of linked rings (with $\mathcal{G} = 1$) is given in Fig. 7(a).

To validate the method we verify first that the distribution functions for $\mathcal{G}$, $P(N;\mathcal{G})$, are symmetric around $\mathcal{G} = 0$ (Fig. S3 in the SM [28]). Then, for $|\mathcal{G}| \geqslant 1$ [57] $P(N;\mathcal{G})$ follows the exponential decay [see Fig. 7(b)]:

$$P(N;\mathcal{G}) \sim e^{-|\mathcal{G}|/\mathcal{G}_0(N)}. \tag{12}$$

The "decay length" $\mathcal{G}_0(N)$ as a function of N (for the specific values, see Table IV) is well described by the power-law behavior [see symbols vs line in the l.h.s. inset (lin-lin plot) and r.h.s. inset (log-log plot) of Fig. 7(b)]:

$$\mathcal{G}_0(N) = \left(\frac{N}{N_{\mathrm{link}}}\right)^{\alpha_{\mathrm{link}}}, \tag{13}$$

with [55]

$$N_{\mathrm{link}} = 5277 \pm 239, \tag{14}$$

$$\alpha_{\mathrm{link}} = 0.363 \pm 0.005. \tag{15}$$

The reported value for α_{link}, close to the scaling exponent ν of the gyration radius of the ring [Fig. 4(a)], is consistent with the intuitive picture that two rings link to each other if the spatial distance between the corresponding centers of mass is of the order or smaller than $R_g(N) \sim N^{\nu}$ [Eq. (5)]. Since $\mathcal{G}_0(N \approx N_{\mathrm{link}}) \approx 1$, N_{link} is intuitively close to the polymer length scale N^* described in Ref. [18] which marks the crossover "from a nonconcatenation contribution to an overlap-dominated concatenation contribution." Although the polymer model adopted here and the one by Lang *et al.* are not the same and a quantitative comparison is difficult, our N_{link} [Eq. (14)] and Lang *et al.*'s N^* [18] are similarly large, in particular of the order of a few thousand bonds.

By using the results on the Gauss linking number, we consider (i) the mean *linking degree* $\langle \mathrm{LD}(N) \rangle$ defined as the mean number of chains linking to a single ring and (ii) the mean ring fraction $\langle M_{\mathrm{cc}}(N) \rangle / M$ belonging to the largest *connected component* of chains in the melt. The results

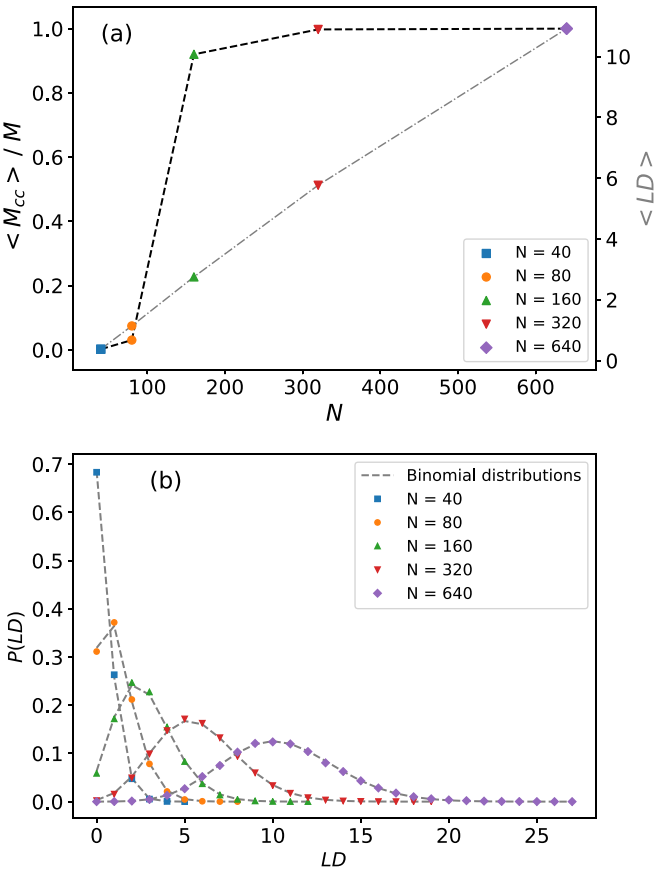

FIG. 8. (a) Mean ring fraction in the largest *connected component* $\langle M_{\mathrm{cc}}(N) \rangle / M$ (black line, left y axis), and mean *linking degree*, $\langle \mathrm{LD}(N) \rangle$ (gray line, right y axis) as a function of N. (b) Frequency of observing a ring linking to, respectively, $\mathrm{LD} = 0, 1, \ldots, M-1$ other rings (symbols) in comparison with the binomial function [lines, Eq. (16)] for random graphs. Color code and symbols are as in Fig. 6(b).

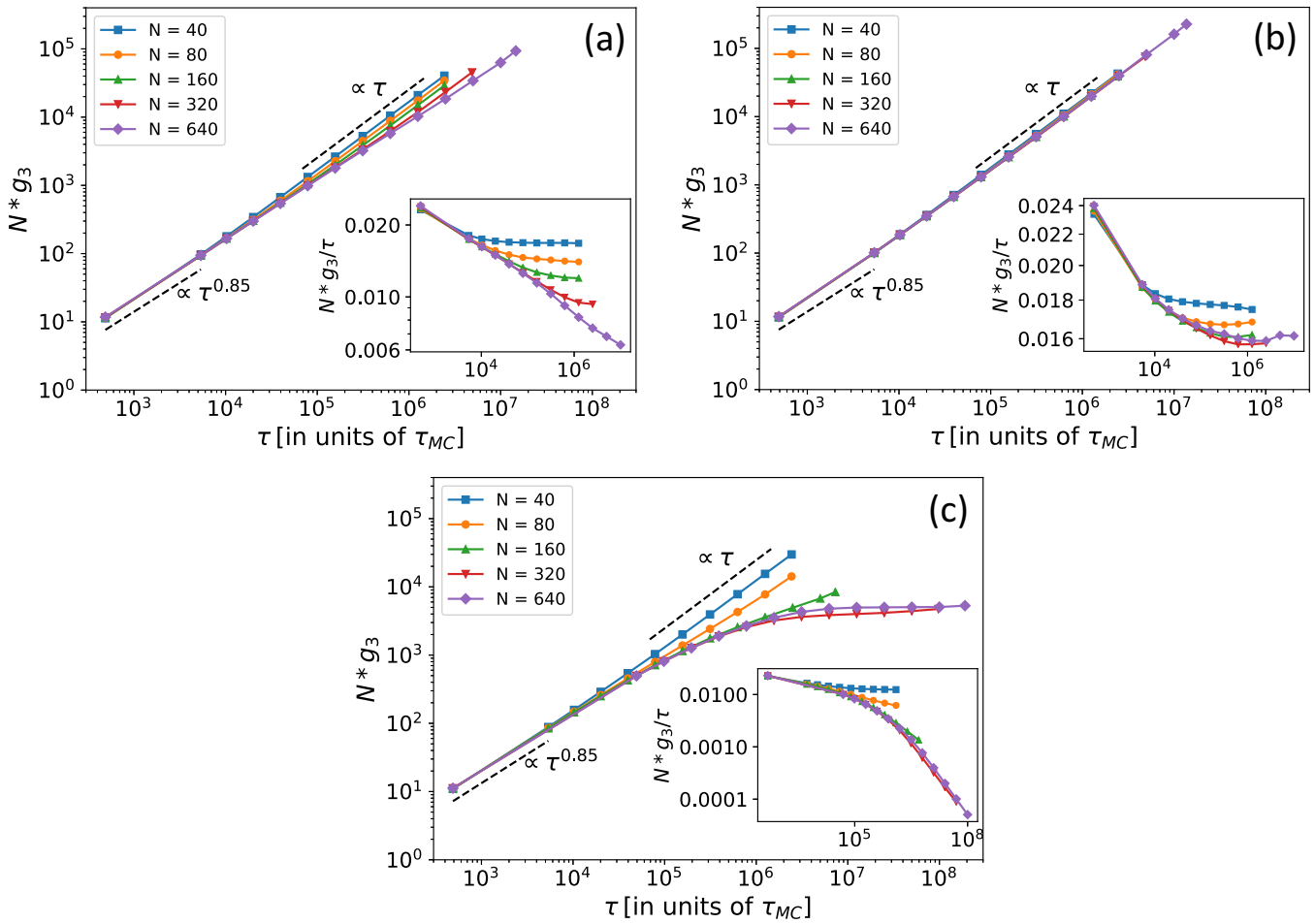

FIG. 9. Time mean-square displacement $g_3(\tau)$ of the center of mass of N-monomer rings in melt. (a) Melts of untangled rings. (b) Melts of rings in the presence of SCs. (c) Melts of permanently catenated rings. The insets display $Ng_3(\tau)/\tau$ as a function of τ. Curves of different colors and with different symbols [color code and symbols are as in Fig. 6(b)] are for different values of N (see legends).

are shown in Fig. 8(a). $\langle \mathrm{LD}(N) \rangle$ increases linearly [18] with N and the largest ($\approx$10) attained value is consistent with the characteristic number of 10–20 chains [7,42] protruding the volume occupied by a single ring in melt. We see that, for $\langle \mathrm{LD}(N) \rangle \gtrsim 2$, i.e., when one ring is connected on average to two (or more) other rings, a single giant network is obtained (see also Fig. S4 in the SM [28] for instantaneous snapshots of the networks for different values of N).

It is interesting to notice that, in agreement with previous studies [21,24], the network of connections has the structure of a *random graph*, hence the frequency of observing a ring linking to, respectively, $\mathrm{LD} = 0, 1, \ldots, M-1$ other rings is accurately described [symbols vs lines in Fig. 8(b)] by the binomial function:

$$P(M, p_{\mathrm{link}}; \mathrm{LD}) = \binom{M-1}{\mathrm{LD}} p_{\mathrm{link}}^{\mathrm{LD}} (1 - p_{\mathrm{link}})^{M-1-\mathrm{LD}}. \quad (16)$$

Equation (16) is equivalent to the probability that a single node in a random graph made of M nodes is connected to LD other nodes, with $p_{\mathrm{link}}(N) = \langle \mathrm{LD}(N) \rangle / (M-1)$ (see values in Table IV) representing the *linking probability* or the fraction of distinct node-to-node links out of the $M(M-1)/2$ total possible combinations. As in Ref. [24], the onset of a single fully connected polymer network can then be interpreted as the *percolation transition* on the graph, signifying that, on average, each node can be reached from any other node by walking on the graph.

2. *Single-chain and network dynamics*

We analyze first the polymer dynamics in the different ensembles. To this purpose, we consider the mean-square displacement of the spatial position $\vec{r}_{\mathrm{c.m.}}(t)$ of the center of mass of the chain [3]:

$$g_3(\tau) \equiv \langle [\vec{r}_{\mathrm{c.m.}}(t+\tau) - \vec{r}_{\mathrm{c.m.}}(t)]^2 \rangle, \quad (17)$$

as a function of time τ.

Unconstrained motion implies that $g_3(\tau) \propto \tau/N$ in the long-time regime. Figure 9(a) shows that this is not the case for untangled rings, in agreement with the original simulations by Schram and Barkema [27]. Conversely, introducing SCs into the system [Fig. 9(b)] removes the constraints and accelerates the dynamics to the extent that $g_3(\tau)$ is now proportional to $1/N$ [Fig. 9(b)]. Then, by the right amount of SCs, it is possible to "fluidize" [15] the entanglements induced by the presence of uncrossable strands and in this way to enhance the dynamics of the polymer system.

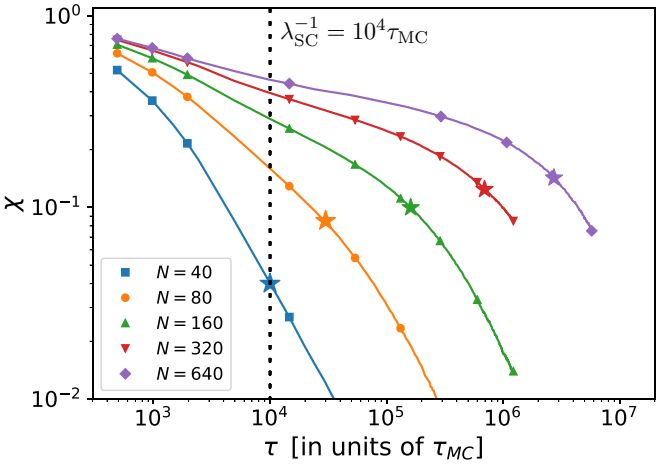

FIG. 10. Time autocorrelation function $\chi(\tau)$ for two rings remaining linked on timescale τ in the presence of SCs [Eq. (18)]. The vertical dotted line corresponds to the timescale $\lambda_{SC}^{-1} = 10^4 \tau_{MC}$ for SC. The "⋆'s" mark the positions of the polymer self-diffusion times $\tau_d(N)$ (see Table I). Color code and symbols are as in Fig. 6(b).

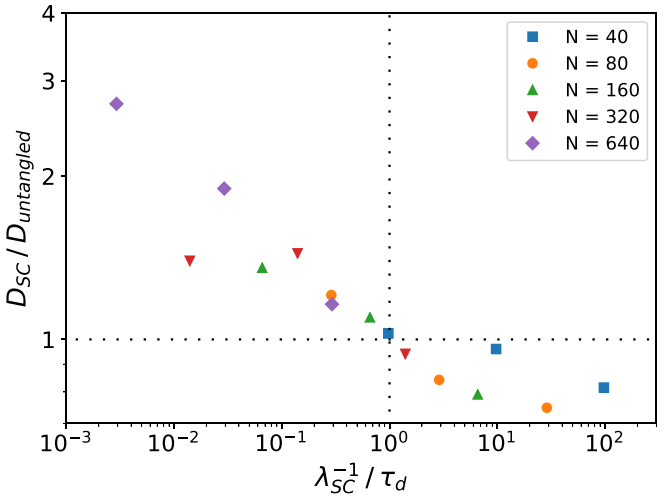

FIG. 11. Asymptotic diffusion coefficient of rings with active SCs normalized to the corresponding values in untangled melts as a function of the inverse of the SC rate, $\lambda_{SC}^{-1}/\tau_d(N)$, normalized to the ring self-diffusion time in untangled melts (see Table I). Color code and symbols are as in Fig. 6(b).

In agreement with that, by again turning off the SC activity and then "quenching" the topology, polymer dynamics slows down dramatically [Fig. 9(c)] up to the complete arrest (evident in the saturation of $g_3(\tau)$ at large times). Slow-down for $N = 40$ and $N = 80$ is due to the fact that rings have linked into multichain structures [Figs. S4(a), S4(b), S5(a), and S5(b) in the SM [28]) which tend to move slower. Starting from $N = 160$ [Figs. S4(c)– S4(e) and S5(c)–S5(e) in the SM [28]] rings are locked together into a single, giant structure and, therefore, unable to perform large-scale diffusion, hence the reported saturation. This effect confirms experimental reports [15] of a rubber-like plateau in the storage modulus of topoII-inactivated solutions of catenated DNA rings. Accordingly, the relative motion displayed by rings with $N = 160$ [line with "▲" symbols, Fig. 9(c)] is the consequence of the fact that a non-negligible amount of unconcatenated rings is still undergoing random diffusion [see Figs. S4(c) and S5(c) in the SM [28]). Notice that these dynamic effects appear on timescales larger than the imposed (Sec. II A) timescale $\lambda_{SC}^{-1} = 10^4 \tau_{MC}$ for SCs: on timescales $\tau \lesssim \lambda_{SC}^{-1}$, the three ensembles show the same subdiffusive behavior $\approx \tau^{0.85}$ characteristic [27] of untangled rings.

To complement the analysis on ring dynamics (Fig. 9) in the presence of active SCs, we characterize now the interplay between ring motion and the "fluidization" [15] process induced by the SC mechanism from the point of view of the formed polymer network. To this purpose, we introduce the characteristic function $C_{ij}^{\rm link}(t) = 1$, $[C_{ij}^{\rm link}(t) = 0]$ between the pair of rings i and j being linked (unlinked) at time t and calculate the corresponding time autocorrelation function:

$$\chi(\tau) \equiv \frac{\langle C_{ij}^{\rm link}(t+\tau) C_{ij}^{\rm link}(t)\rangle}{\langle C_{ij}^{\rm link}(t)^2\rangle}, \qquad (18)$$

where the average is taken over all possible pairs i and j. The results for rings made of N monomers are shown in Fig. 10. Qualitatively, we identify three regimes: (i) Below the SC timescale $\lambda_{SC}^{-1} = 10^4 \tau_{MC}$, $\chi(\tau)$ displays a power-law decay. (ii) This is followed by a second regime which, by increasing N, becomes slower than the first one and attains a quasiplateau. Intuitively, this is due to the fact that, on such timescales, both linking and unlinking events may happen, while at times $\tau < \lambda_{SC}^{-1}$ we expect on average only a single unlinking event. (iii) Finally, on timescales larger than the ring self-diffusion time $\tau_d(N)$ [corresponding to the timescale for the polymer to spread over a distance the size of its own mean gyration radius, $g_3(\tau_d(N)) \equiv \langle R_g^2(N)\rangle$, see Table I], the two rings occupy, on average, distinct regions in space and $\chi(\tau)$ decays as an exponential. The "persistent" regime (ii) valid for long chains is particularly noteworthy, because it suggests that, with SCs, work rings coalesce into a "dynamic" gel-like structure.

IV. DISCUSSION

Our melts of rings with active SCs form transient networks (Fig. 10) which, in spite of the non-negligible amount of introduced linking (Fig. 7), move faster than in the untangled case [Fig. 9(a) vs 9(b)]. Physically this happens because SCs operate at a reasonably fast rate ($\lambda_{SC}^{-1} = 10^4 \tau_{MC}$, see Sec. II A), guaranteeing rapid linking and unlinking events which maintain rings only "loosely" entangled with each other.

By the same argument one may imagine that, by opportunely slowing down the SC rate λ_{SC}, it ought to be possible to create systems of interlocked rings where topological constraints are temporary yet long-lived [58]: as a consequence, now chain dynamics is expected to be *slower* than in untangled melts [59]. Intuitively this situation can be realized by choosing λ_{SC}^{-1} to be of the same order or larger than the self-diffusion time τ_d of rings in untangled melts since, supposedly, during this timescale a single polymer has interacted with the chains to which it is effectively able to link.

To validate this idea (which may be also tested experimentally, for instance by resorting to DNA rings [15]), we performed new simulations for the same melts of rings but

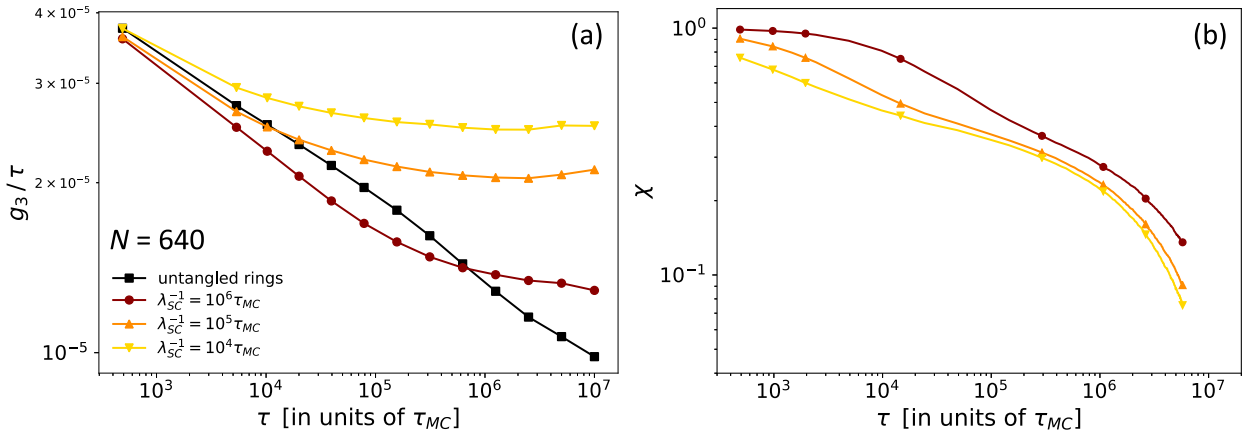

FIG. 12. (a) $g_3(\tau)/\tau$: time mean-square displacement of the center of mass of rings with $N = 640$ monomers normalized to time τ. (b) $\chi(\tau)$: time-correlation function for two rings remaining linked on time span τ in the presence of SCs [Eq. (18)]. Different colors and symbols are for different SC rates λ_{SC} (see legend).

with the two different rates $\lambda_{SC}^{-1} = 10^5\tau_{MC}$ and $\lambda_{SC}^{-1} = 10^6\tau_{MC}$, i.e., ten and one hundred times slower than the previous one. We have then estimated the asymptotic diffusion coefficients of the rings, D_{SC}, by best fits of the terminal behavior of the corresponding mean-square displacements, $g_3(\tau)/\tau$ (see Fig. S6 in the SM [28]), normalized to time τ. The results (normalized to the corresponding values for untangled melts, $D_{untangled}$) vs the inverse of the SC rate, $\lambda_{SC}^{-1}/\tau_d(N)$, normalized to the polymer self-diffusion times in untangled melts are shown in Fig. 11. The plots confirm our expectations: slow SC rates result in melts with slower relaxation dynamics compared with the untangled case. Notice that, while the precise value of the SC rate affects the dynamics of the melt, static quantities like the gyration radius of the ring or the Gauss linking number (see, respectively, Figs. S7 and S8 in the SM [28]) do not change for the different setups.

It is also worth noticing that, even in those cases where SC accelerates the asymptotic chain dynamics with respect to the untangled case, detailed analysis of $g_3(\tau)/\tau$ shows a regime where the action of SCs makes the rings temporarily slower [Fig. 12(a), the "$\lambda_{SC}^{-1} = 10^6\tau_{MC}$" curve vs the untangled case for $N = 640$ and on timescales $\tau/\tau_{MC} \lesssim 10^5$]. On the same timescales, the time autocorrelation function $\chi(\tau)$ for link dynamics [Eq. (18), see corresponding lines in Fig. 12(b)] becomes increasingly slower with λ_{SC}^{-1}, demonstrating that the observed polymer slows down compared with the untangled case is the consequence of persistent links between rings.

V. CONCLUSIONS

Motivated by recent experiments [15] employing the enzyme topoII to induce "fluidization" of the topological constraints arising in entangled solutions of DNA rings, we have introduced a dynamic Monte Carlo computational scheme for polymer chains on the fcc lattice which takes explicitly into account the action of the enzyme by controlling the rate at which two nearby polymer strands are able to cross through each other. By applying then the model to ring polymers made of N monomers and in melt conditions, we discuss how the strand-crossing mechanism influences both the static and the dynamic properties of the chains.

At stationary conditions, ring polymers swell with respect to the untangled (i.e., unknotted and unconcatenated) case and stay nonideal (Fig. 4). On the other hand, they tend to become increasingly knotted (Fig. 6) and to form a macroscopic network of linked chains (Figs. 7 and 8). As a byproduct, yet quite intriguingly, we find (Fig. 6, insets) that the knotting probability $P_{knot}(N)$ increases with N more sharply than in other analogous studies. We conjecture that this is due to the fact that knots form through the random crossings between *pairs* of polymer strands, and we point out that it would be worth investigating this question more systematically by simulating ring polymers of much larger contour length (for instance, by adapting the efficient GPU-based implementation of the original lattice model described in Ref. [27]).

On the dynamics side, we show (Fig. 9) that the ability to produce strand crossings make polymers faster and that large rings tend to "glue" together into a permanent gel as soon as crossings are not allowed anymore. Yet an acceleration of the dynamics is not true *in general*, but only when the rate for strand crossings is fast enough. In the opposite case, the dynamics of the melt may be even slower than the untangled case (Fig. 11), a prediction which might be tested by using, again, DNA rings in the presence of topoII.

We conclude on a technical remark. Notice that the model presented here is for flexible chains (Sec. II E) while polymers in general, and DNA in particular [60], are typically semiflexible i.e., locally stiff [8]. The inclusion of a bending penalty term in our model is not presenting particular technical difficulties and its consequences on the topological properties of ring polymers will be examined in future studies.

ACKNOWLEDGMENTS

The authors would like to acknowledge the networking support by the "European Topology Interdisciplinary Action" (EUTOPIA) CA17139.

[1] M. Doi and S. F. Edwards, *The Theory of Polymer Dynamics* (Clarendon, Oxford, 1986).
[2] P. G. de Gennes, J. Chem. Phys. **55**, 572 (1971).
[3] K. Kremer and G. S. Grest, J. Chem. Phys. **92**, 5057 (1990).
[4] M. E. Cates and J. M. Deutsch, J. Phys. (Paris) **47**, 2121 (1986).
[5] J. D. Halverson, W. B. Lee, G. S. Grest, A. Y. Grosberg, and K. Kremer, J. Chem. Phys. **134**, 204904 (2011).
[6] A. Y. Grosberg, Soft Matter **10**, 560 (2014).
[7] A. Rosa and R. Everaers, Phys. Rev. Lett. **112**, 118302 (2014).
[8] M. Rubinstein and R. H. Colby, *Polymer Physics* (Oxford University Press, New York, 2003).
[9] Q. Wu, P. M. Rauscher, X. Lang, R. J. Wojtecki, J. J. de Pablo, M. J. A. Hore, and S. J. Rowan, Science **358**, 1434 (2017).
[10] L. F. Hart, J. E. Hertzog, P. M. Rauscher, B. W. Rawe, M. M. Tranquilli, and S. J. Rowan, Nat. Rev. Mater. **6**, 508 (2021).
[11] T. Cremer and C. Cremer, Nat. Rev. Genet. **2**, 292 (2001).
[12] S. Brahmachari and J. F. Marko, Proc. Natl. Acad. Sci. USA **116**, 24956 (2019).
[13] J. J. Champoux, Annu. Rev. Biochem. **70**, 369 (2001).
[14] J. L. Sikorav and G. Jannink, Biophys. J. **66**, 827 (1994).
[15] B. A. Krajina, A. Zhu, S. C. Heilshorn, and A. J. Spakowitz, Phys. Rev. Lett. **121**, 148001 (2018).
[16] P. G. de Gennes, *Scaling Concepts in Polymer Physics* (Cornell University Press, Ithaca and London, 1979).
[17] E. Raphaël, C. Gay, and P. G. de Gennes, J. Stat. Phys. **89**, 111 (1997).
[18] M. Lang, J. Fischer, and J. U. Sommer, Macromolecules (Washington, DC, U. S.) **45**, 7642 (2012).
[19] M. Lang, J. Fischer, M. Werner, and J.-U. Sommer, Phys. Rev. Lett. **112**, 238001 (2014).
[20] M. Lang, J. Fischer, M. Werner, and J.-U. Sommer, Macromol. Symp. **358**, 140 (2015).
[21] J. Fischer, M. Lang, and J.-U. Sommer, J. Chem. Phys. **143**, 243114 (2015).
[22] H. C. Renger and D. R. Wolstenholme, J. Cell Biol. **54**, 346 (1972).
[23] A. R. Klotz, B. W. Soh, and P. S. Doyle, Proc. Natl. Acad. Sci. USA **117**, 121 (2020).
[24] D. Michieletto, D. Marenduzzo, and E. Orlandini, Phys. Biol. **12**, 036001 (2015).
[25] Y. S. Kim, B. Kundukad, A. Allahverdi, L. Nordensköld, P. S. Doyle, and J. R. C. van der Maarel, Soft Matter **9**, 1656 (2013).
[26] V. Hugouvieux, M. A. V. Axelos, and M. Kolb, Macromolecules (Washington, DC, U. S.) **42**, 392 (2009).
[27] R. D. Schram and G. T. Barkema, J. Comput. Phys. **363**, 128 (2018).
[28] See Supplemental Material at http://link.aps.org/supplemental/10.1103/PhysRevE.104.054503 for the additional figures.
[29] Our work is based on the original polymer model [26,27]. As explained in Ref. [26], the choice of the fcc lattice "is motivated by a greater number of nearest neighbors (12) and a wider and smoother range of bonding angles than a standard cubic (6) lattice.".
[30] M. Rubinstein, Phys. Rev. Lett. **59**, 1946 (1987).
[31] A similar move was introduced in Ref. [61] with the purpose of accelerating the equilibration of long polymer chains on the fcc lattice and investigating the structural stability of the so called *fractal globule* [46]. The authors' choice, however, does not necessarily modify topology (which is, instead, the main concern here) and the paper did not address questions like the physical consequences of using different strand-crossing rates (Sec. II B).
[32] R. D. Schram, A. Rosa, and R. Everaers, Soft Matter **15**, 2418 (2019).
[33] J. S. Shaffer, J. Chem. Phys. **101**, 4205 (1994).
[34] J. S. Shaffer, J. Chem. Phys. **103**, 761 (1995).
[35] S. Brown, T. Lenczycki, and G. Szamel, Phys. Rev. E **63**, 052801 (2001).
[36] I. Carmesin and K. Kremer, Macromolecules (Washington, DC, U. S.) **21**, 2819 (1988).
[37] W. Paul, K. Binder, D. W. Heermann, and K. Kremer, J. Phys. II **1**, 37 (1991).
[38] M. Tanaka, K. Iwata, and N. Kuzuu, Comput. Theor. Polym. Sci. **10**, 299 (2000).
[39] R. Auhl, R. Everaers, G. S. Grest, K. Kremer, and S. J. Plimpton, J. Chem. Phys. **119**, 12718 (2003).
[40] N. Uchida, G. S. Grest, and R. Everaers, J. Chem. Phys. **128**, 044902 (2008).
[41] H.-P. Hsu, W. Paul, and K. Binder, Macromolecules (Washington, DC, U. S.) **43**, 3094 (2010).
[42] T. Ge, S. Panyukov, and M. Rubinstein, Macromolecules (Washington, DC, U. S.) **49**, 708 (2016).
[43] Y. H. Lin, Macromolecules (Washington, DC, U. S.) **20**, 3080 (1987).
[44] T. A. Kavassalis and J. Noolandi, Phys. Rev. Lett. **59**, 2674 (1987).
[45] T. Minato and A. Hatano, J. Phys. Soc. Jpn. **42**, 1992 (1977).
[46] E. Lieberman-Aiden, N. L. van Berkum, L. Williams, M. Imakaev, T. Ragoczy, A. Telling, I. Amit, B. R. Lajoie, P. J. Sabo, M. O. Dorschner, R. Sandstrom, B. Bernstein, M. A. Bender, M. Groudine, A. Gnirke, J. Stamatoyannopoulos, L. A. Mirny, E. S. Lander, and J. Dekker, Science **326**, 289 (2009).
[47] A. Rosa, N. B. Becker, and R. Everaers, Biophys. J. **98**, 2410 (2010).
[48] J. D. Halverson, J. Smrek, K. Kremer, and A. Y. Grosberg, Rep. Prog. Phys. **77**, 022601 (2014).
[49] A. Rosa and R. Everaers, Eur. Phys. J. E: Soft Matter Biol. Phys. **42**, 1 (2019).
[50] Neglecting excluded-volume correlations [48], the contact probability between two monomers is simply proportional to the inverse of the spanned volume, or $\gamma = 3\nu$.
[51] C. Micheletti, D. Marenduzzo, and E. Orlandini, Phys. Rep. **504**, 1 (2011).
[52] E. Orlandini and S. G. Whittington, Rev. Mod. Phys. **79**, 611 (2007).
[53] L. Tubiana, G. Polles, E. Orlandini, and C. Micheletti, Eur. Phys. J. E: Soft Matter Biol. Phys. **41**, 72 (2018).
[54] A. Y. Grosberg, Phys. Rev. Lett. **85**, 3858 (2000).
[55] Mean values and corresponding error bars for $N_{\rm knot}$ and $\alpha_{\rm knot}$ [Eq. (8)] were calculated by averaging distinct estimates of these parameters. These estimates were obtained by separate best fits of the data to Eq. (8) in the linear-linear and log-log representations. The same procedure was used for $N_{\rm link}$ and $\alpha_{\rm link}$ [Eq. (13)].
[56] K. Klenin and J. Langowski, Biopolymers **54**, 307 (2000).
[57] Notice that since $\mathcal{G}$ has been computed between all possible ring pairs, the value for $P(N;\mathcal{G}=0)$ does depend on the total number of chains in the sample (in an infinite system, there is an infinite number of unlinked chains). Conversely, two chains are linked only if they are spatially close to each other and so

each value $P(N;\mathcal{G} \geqslant 1)$ is expected to correspond to "bulk" properties.

[58] E. Lee and Y. Jung, Polymers (Basel, Switz.) **11**, 516 (2019).

[59] Notice that since, in the absence of the SC mechanism, rings must follow untangled dynamics, this is equivalent to saying ring diffusivities display non-monotonous behavior as a function of λ_{SC}.

[60] J. F. Marko and E. D. Siggia, Macromolecules (Washington, DC, U. S.) **28**, 8759 (1995).

[61] R. D. Schram, G. T. Barkema, and H. Schiessel, J. Chem. Phys. **138**, 224901 (2013).